PCCP

Accepted Manuscript

This article can be cited before page numbers have been issued, to do this please use: S. C. Perry and G. Denuault, *Phys. Chem. Chem. Phys.*, 2016, DOI: 10.1039/C6CP00106H.

ROYAL SOCIETY OF CHEMISTRY

www.rsc.org/pccp

View Article Online
DOI: 10.1039/C6CP00106H

Journal Name

ARTICLE

The oxygen reduction reaction (ORR) on reduced metals: evidence for a unique relationship between the coverage of adsorbed oxygen species and adsorption energy

Received 00th January 20xx,
Accepted 00th January 20xx

DOI: 10.1039/x0xx00000x

www.rsc.org/

S. C. Perry[‡] and G. Denuault[*]

Using chronoamperometry and voltammetry at oxide-free microelectrodes in non-adsorbing electrolyte, $KClO_4$, we investigated the reduction of oxygen containing species which adsorb at potentials below those where oxides are grown electrochemically when the electrode is exposed to dissolved oxygen. Their coverage is found to vary with the metal substrate as follows, Ni > Cu > Pt > Ag, and is negligible on Au microdiscs. This dependence is consistent with the adsorption energy of atomic oxygen for the respective metals predicted by DFT. Furthermore the adsorption energies derived from the stripping peak potentials for the different metals agree very well with those predicted by the DFT calculations. We exploit the oxygen coverage differences between Pt, $Pt_{0.9}Rh_{0.1}$ and $Pt_{0.9}Ir_{0.1}$ microdiscs to predict the adsorption energy of these species on the Pt alloys and demonstrate a clear correlation between the metal activity towards the ORR and the charge associated with the reduction of the adsorbed oxygen species. In effect the coverage - adsorption energy relationship turns the charge associated with the reduction of the adsorbed oxygen species into a descriptor of the electrode activity towards the ORR. This study provides new insight into the oxygen reduction reaction and offers a new methodology to investigate low temperature fuel cell ORR catalysts.

Introduction

The slow kinetics of the oxygen reduction reaction limits the commercialisation of low temperature fuel cells and great efforts are being made to develop active and affordable cathode materials. However, the reaction is complex and a detailed reaction mechanism is still a long way off, even on the most electroactive materials, supported Pt, Pt alloys or core shell Pt nanoparticles, and single crystal Pt surfaces.[1] The overall mechanism[2] reflects the cleavage of the oxygen bond, the adsorption and desorption of intermediates and the transfer of four electrons and four protons but the elementary steps, the rate determining step and the nature of the adsorbed intermediates are still debated.[3-8] Adsorbed oxygen containing species are generally considered as the most likely intermediates[9] but the existence of soluble radical intermediates has also been reported.[4, 10, 11] Recent theoretical investigations link the ORR activity to the coverage of adsorbed oxygen containing species and to their adsorption energy with respect to the metal substrate.[6, 12]

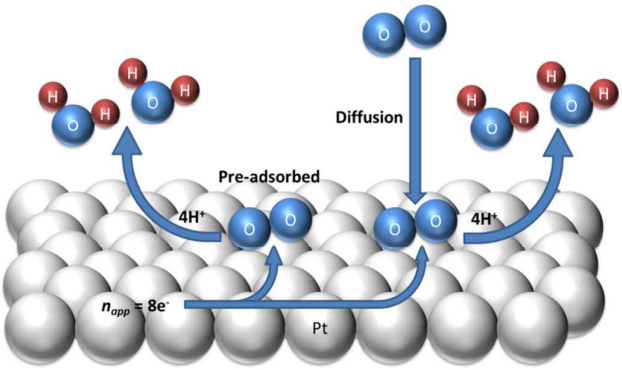

Scheme 1: The reduction of pre-adsorbed oxygen species briefly occurs in parallel with the reduction of oxygen arriving from the bulk of the solution until all the pre-adsorbed oxygen species have been consumed.

Using suitably preconditioned Pt microdisc electrodes we investigated the oxygen reduction reaction on sub-second timescales and observed the reduction of oxygen containing species which adsorb at potentials below those where Pt oxides are grown electrochemically but only when the electrode is exposed to oxygen in solution.[13] We found that the reduction of these adsorbed oxygen species was distinct from that of dissolved oxygen as schematically presented in scheme 1. We also showed that it is possible to control and monitor their coverage and that the experimental protocol was sufficiently sensitive to distinguish between adsorption on

Chemistry, University of Southampton, Southampton, SO17 1BJ, UK.
‡ now at Chemistry Department, McGill University,801 Sherbrooke Street West, Montreal, H3A 0B8, Canada
Email: gd@soton.ac.uk

† Electronic Supplementary Information (ESI) available: Voltammograms, Potentiostatic waveforms, Chronoamperograms and Cottrell plots, Estimation of the adsorption energies, of the electrode electroactive area and of the oxygen coverage, ORR kinetic currents. See DOI: 10.1039/x0xx00000x

View Article Online
DOI: 10.1039/C6CP00106H

Pt, $Pt_{0.9}Ir_{0.1}$ and $Pt_{0.9}Rh_{0.1}$. These oxygen species are clearly linked to the presence of molecular oxygen in solution as their reduction was only observed after exposing the electrode to dissolved oxygen and their coverage systematically increased with the bulk oxygen concentration before reaching a saturation plateau.[13] While these results are consistent with observations in the gas phase where a number of studies have reported that molecular oxygen irreversibly dissociates upon adsorption on metal surfaces,[14-16] at solid-liquid interfaces it is experimentally difficult, without transfer of the electrode to UHV, to detect and identify the adsorbed oxygen species. However our results are congruous with recent electrochemical quartz microbalance data[17, 18] which show the mass increasing after switching from a He to O_2 saturated solution prior to the ORR then decreasing during the ORR.

In the present article we provide further experimental evidence which demonstrates that the adsorbed oxygen species are distinct from the oxides grown electrochemically and we show significant variations of their coverage with a range of metal substrates on either side of the volcano plot for ORR activity. For each metal we experimentally determine the adsorption energy of these oxygen species and compare it with published values. To illustrate possible applications we use the coverage recorded on the Pt alloys to predict oxygen adsorption energy on these substrates and we describe how the coverage can be exploited as a proxy to predict the substrate activity towards the ORR.

Experimental section

Experiments were conducted as previously described.[13] Briefly, 0.1 M $KClO_4$ (99%, Sigma-Aldrich) solutions prepared with ultrapure water (18 MΩ cm, Purite, Burkert) were aerated by bubbling humid air, or deaerated by bubbling humid Ar (Pureshield, BOC), through a glass frit for 30 min. Air and Ar were scrubbed and humidified by passing through a Drechsel bottle filled with 0.1 M $KClO_4$. The jacketed cell was thermostated at 25 °C with a water bath (Grant W14), placed inside a grounded Faraday cage and all water tubing was screened with a grounded metal wire mesh. All glassware was soaked overnight in 5% Decon 90 (BHD) and rinsed several times with ultrapure water before use. All experiments were carried out with a two electrode configuration. Microelectrodes were homemade with 99.99% annealed wires from Goodfellow and their radius was determined with an electron microscope (XL30 ESEM, FEI). They were regularly polished with 0.3 µm alumina powder (Buehler) on a polishing Microcloth (Buehler) and cycled at 200 mV s^{-1} in the electrolyte until a stable voltammogram was seen (typical voltammograms are shown in ESI†). The reference electrode was either a homemade saturated calomel reference electrode or a homemade saturated mercurous sulphate electrode to avoid chloride traces. All potentials are quoted with respect to the reversible hydrogen electrode (RHE). The electrodes were connected to a PGSTAT101 Autolab operated with NOVA 1.10 (Ecochemie). Bubbling with humid air and maintaining a constant cell temperature made it possible to control the oxygen solubility and diffusion coefficient. The oxygen concentration was corrected for variations in atmospheric pressure as described previously[13] and its diffusion coefficient was determined as reported previously.[19]

The working electrodes were systematically preconditioned potentiostatically to obtain reproducible results and to ensure each experiment started with a reduced surface free from oxides. The preconditioning waveform was as previously described[13, 20] but the upper cleaning, rest and lower cleaning potentials were adjusted for each metal substrate as listed in table SI-1 (ESI†). Briefly the electrode was cleaned by sweeping between upper and lower cleaning potentials at 500 mV s^{-1} six times. The potential was then held for 10 s at the previously determined open circuit potential (OCP) and then stepped to the ORR plateau for 0.5 s to record the chronoamperometric response or swept at 100 mV s^{-1} to record the ORR wave. The potential was then returned to the OCP for the next experiment. The upper cleaning potential was set to oxidise the surface without increasing its roughness and the lower cleaning potential was set to remove the oxides and adsorb hydrogen. The rest potential was always reached from the lower cleaning potential to ensure the electrode surface was reduced and free from oxide. All experiments were conducted with microdisc electrodes to avoid double layer distortion and to benefit from the well-defined diffusional properties.[21, 22] To control the presence of oxygen, experiments were performed by switching between aerated and Ar purged solutions at different stages of the waveform and then comparing the voltammograms recorded in aerated solutions, in Ar purged solutions and after purging with Ar at the end of the rest.

Results and discussion

Fig. 1 shows typical linear sweep voltammograms (LSV) recorded with a Pt microdisc. The black line was obtained after conditioning and resting the electrode in aerated solution, purging the solution with Ar for 20 min while holding the electrode at the rest potential then sweeping in deaerated conditions; the potential waveform is shown in Fig. SI-9 (ESI†). The background LSV, red line, was recorded after conditioning, resting and sweeping the electrode in deaerated solution; the corresponding waveform is shown in Fig. SI-7 (ESI†). Allowing the electrode to rest in presence of oxygen clearly produces extra current and the background subtracted LSV, blue line, has the characteristic peak-shape observed for a redox species adsorbed on the electrode. Integrating the area under the peak yields a charge of 0.55 nC equating to 37.9 µC cm^{-2} of electroactive area. This charge is similar to that determined by chronoamperometry in aerated solution after subtracting the diffusion controlled response for the ORR and we have shown that it increases with the rest time and dissolved oxygen concentration before reaching a plateau.[13] In effect the coverage of adsorbed oxygen species can be controlled through the rest time and the bulk concentration of dissolved oxygen. In our previous study we also showed that this charge is clearly related to the availability of adsorption sites on the electrode since it decreases systematically in the order ClO_4^- >

View Article Online
DOI: 10.1039/C6CP00106H

Cl^- > Br^- > I^- when switching to increasingly adsorbing electrolytes.

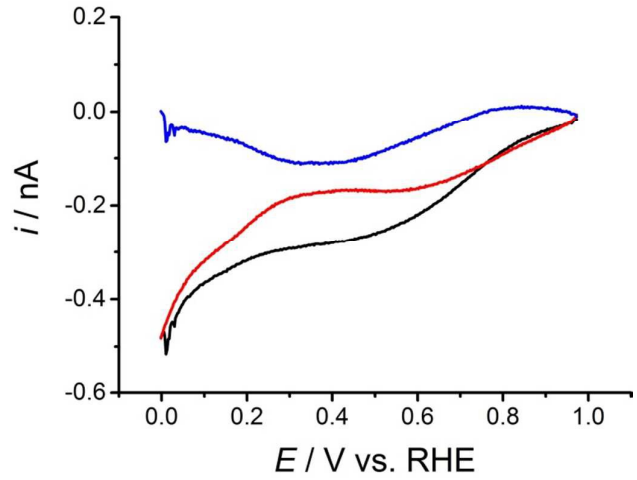

Fig. 1: Linear sweep voltammograms recorded in 0.1 M $KClO_4$ with a 25 µm Ø Pt disc at 100 mV s^{-1} from 1.0 V (OCP) to 0 V vs. RHE after conditioning the electrode and resting at OCP for 10 s in aerated solution then purging the solution with argon (—), after conditioning the electrode and resting at OCP for 10 s in Ar purged solution (—). Subtraction of the latter from the former yields the background subtracted LSV (—).

The processes behind the background current are not all clear. Below 0.3 V the current reflects the onset of hydrogen adsorption but the plateau between 0.3 and 0.6 V is not due to the diffusion controlled reduction of trace impurities because the current transient recorded after conditioning, resting at OCP and stepping the potential to 0.4 V in Ar purged solution does not fit the theoretical diffusion controlled current to a microdisc electrode.[23] The reduction of oxygen traces is also unlikely because experiments performed in presence of Na_2SO_3 produced similar background currents.

In Fig. 2 we demonstrate that the oxygen species that adsorb on the electrode surface during the rest are distinct from the Pt oxides grown electrochemically. The black curve is the background subtracted LSV shown in Fig. 1 and corresponds to a rest at OCP, 1.0 V vs. RHE. In contrast the red curve is the background subtracted LSV obtained when the rest potential was set at 1.5 V, a value sufficiently positive to drive the growth of Pt oxides. These were grown in absence of oxygen and with a similar rest time of 10 s; the corresponding waveform is shown in Fig. SI-10 (ESI†). Both curves show characteristic Gaussian peaks consistent with the stripping of surface species but the peak potential for the oxides grown at 1.5 V is circa 200 mV more positive than that for the species adsorbed at 1.0 V. The position of the oxide reduction peak is not specific to the conditions used here as it appears at the same potential on a cyclic voltammogram recorded in absence of oxygen, Fig. SI-1 (ESI†). The large peak potential difference suggests that the species involved are different and this is in accord with our previous chronoamperometric experiments[13] where the charge for the reduction of the adsorbed species was linearly related to the rest potential above 1.05 V, a feature characteristic of Pt oxides growth,[24-26] but independent of the rest potential below this value. The 200 mV difference could arise from a large local acidification during the growth of the oxides but this is unlikely because the protons released diffuse away from the microdisc rapidly and the local pH would have to decrease below 4 (compared to 7.34 in the bulk) for the oxide stripping peak to shift positively by 200 mV.

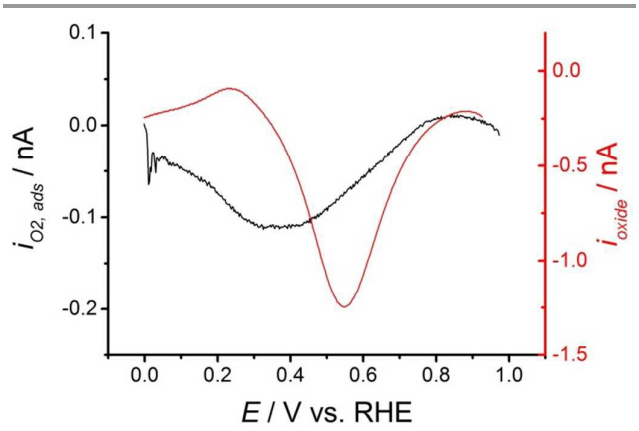

Fig. 2: Background subtracted linear sweep voltammograms recorded in 0.1 M $KClO_4$ with a 25 µm Ø Pt disc at 100 mV s^{-1} from 1.0 V (OCP) to 0 V vs. RHE after conditioning the electrode then allowing adsorption of oxygen species. (Black) the electrode was rested at OCP i.e. 1.0 V vs. RHE for 10 s in aerated solution before purging with Ar for 20 min. (Red) the electrode was rested at 1.5 V vs. RHE for 10 s in an already degassed solution. In each case the background voltammogram was recorded after conditioning, resting (1.0 V vs. RHE) and sweeping in Ar purged solution.

We previously reported that the charge associated with the reduction of the adsorbed oxygen species depends on the metal substrate and that it is sufficiently reproducible to distinguish coverage differences between Pt, $Pt_{0.9}Rh_{0.1}$ and $Pt_{0.9}Ir_{0.1}$.[13] We now provide the results of experiments conducted with Au, Ag, Cu and Ni microdiscs. These metals were specifically chosen to offer a range of adsorption energies towards oxygen since theoretical calculations predict binding strengths increasing in the order: Au < Ag < Pt < Cu < Ni.[27] Each microdisc was conditioned as for Pt but with potentials specifically adapted to each metal as shown in Table SI-1. Relevant voltammograms and conditioning waveforms are also shown in ESI†. Except for Au, all microelectrodes produced oxygen reduction currents larger than the expected diffusion controlled response at short times. The chronoamperograms, Fig. SI-11 (ESI†), were treated as previously reported[13] by subtracting the diffusion controlled current and the resulting current was integrated with respect to time to produce the corresponding charge. For the Au, Ag, Pt, Cu and Ni microdiscs the charges were respectively 0.4±0.0, 12±4, 54±2, 142±4 and 185±7 µC cm^{-2}. Similar experiments respectively yielded charges of 39±2 and 29±1 µC cm^{-2} with $Pt_{0.9}Rh_{0.1}$ and $Pt_{0.9}Ir_{0.1}$ microdiscs.[13] Together these results reveal a strong and sensitive dependence of the charge on the metal substrate, furthermore the dependence is consistent with the trend in adsorption energies predicted by DFT.[27]

Assuming one oxygen atom per metal atom, a four electron process and a similar roughness for all surfaces, the above charges respectively correspond to 0, 0.04, 0.06, 0.09, 0.12, 0.23 and 0.33 monolayers for Au, Ag, PtIr, PtRh, Pt, Cu

View Article Online
DOI: 10.1039/C6CP00106H

and Ni; relevant calculations are given in ESI†. Whilst these values should be treated with caution in view of the assumptions made, it is still worth noting that the coverage is low in most cases.

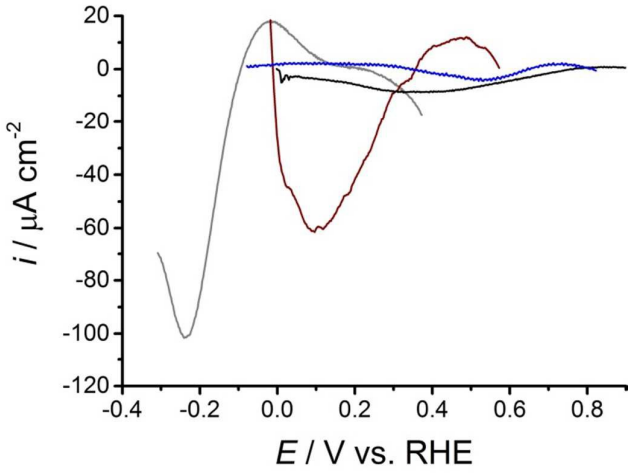

Fig. 3: Background subtracted stripping voltammograms recorded with 25 µm Ø Ni (grey), Cu (brown), Pt (black) and Ag (blue) electrodes in 0.1 M $KClO_4$. In each case the electrode was first conditioned and rested at OCP in aerated solution. The solution was then purged with Ar and the first potential sweep was run from OCP. The electrode was then reconditioned and allowed to rest at OCP and a second sweep was performed. In both cases the scan rate was 100 mV s^{-1}. The second voltammogram was subtracted from the first to remove the background.

To complement the chronoamperometry linear sweep voltammograms were recorded with each microdisc (except the gold one since the charge found on Au is negligible) and adsorption energies of the oxygen species towards the respective metals were derived from the striping peak potential. In these experiments each electrode was conditioned and rested in aerated $KClO_4$ as before. At the end of the rest the solution was purged with Ar for 20 min to remove oxygen from the bulk. The potential was then swept at 100 mV s^{-1} from the OCP to reduce the layer of oxygen species. The electrode was then reconditioned and rested at OCP in the Ar purged solution and a second linear sweep voltammogram was recorded to acquire the background. Note that the stripping voltammograms were recorded at low sweep rates to avoid the kinetic distortions observed at short time scales[13] which would have shifted the peak to lower potentials thereby artificially increasing the adsorption energies. The latter were calculated from the difference between the stripping peak potential and the thermodynamic potential for the ORR corrected for the pH of the solution (7.34) assuming two electrons per oxygen atom, see details in ESI†. Fig. 3 shows the resulting background subtracted linear sweep voltammograms obtained with the different microelectrodes. At pH 7.34 the thermodynamic potential for the ORR is circa 0.8 V vs. RHE so the peak potentials clearly indicate that reducing the layer of adsorbed oxygen species is the easiest on the Ag microdisc and the hardest on the Ni microdisc. In agreement with the chronoamperometric results, the peak areas reveal that the oxygen species coverage increases in the order Ag < Pt < Cu < Ni. Although it is possible to estimate the charge under each peak, these peak areas were not used for quantitative analysis because of the large uncertainty associated with the choice of integration limits and baseline. Instead the charges were derived from the integrated difference between experimental and theoretical current transients for the oxygen reduction reaction because this approach yields very reproducible results.

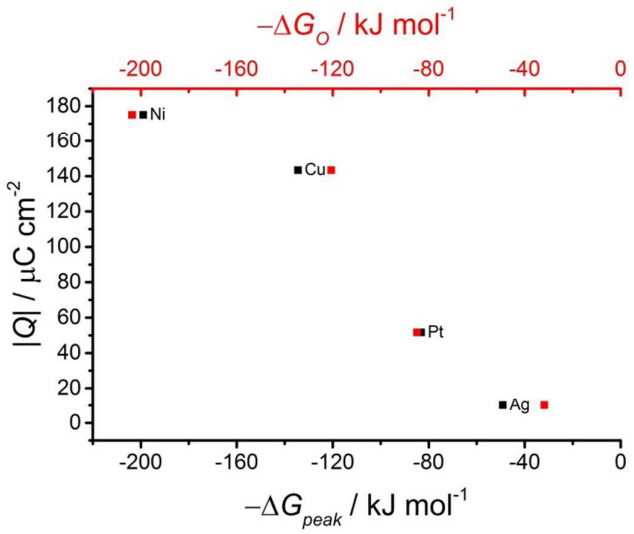

Fig. 4: Charge calculated from the integrated difference between experimental and theoretical current transients for the oxygen reduction reaction at Ni, Cu, Pt, and Ag 25 µm Ø microdiscs in aerated 0.1 M $KClO_4$. The horizontal axes show the adsorption energy of oxygen species for the respective metals obtained from stripping voltammograms (bottom axis and black squares) and DFT calculations (top axis and red squares) taken from ref.[27]

In Fig. 4 the extra charge found for each electrode is plotted against the adsorption energy derived from the stripping peak potentials, bottom axis, and the adsorption energy from published DFT calculations,[27] top axis. A unique trend is revealed whereby stronger affinity towards oxygen adsorption results in a larger charge, i.e. in a larger coverage of adsorbed oxygen species. Another important observation arising from Fig. 4 is that the experimental adsorption energies are in remarkable agreement with the theoretical adsorption energies from DFT. The unique relationship shown in Fig. 4 can in fact be used as a calibration curve as illustrated in Fig. 5 where the line drawn between the points has no theoretical basis and is only intended as a guide. For example the stripping voltammograms recorded with the two Pt alloy microdiscs had very broad peaks which made it difficult to accurately determine their peak potential but they appeared between Ag and Pt thereby indicating that the small amount of Ir or Rh had lowered the adsorption energy of oxygen compared to bulk Pt. Reporting their extra charge on the graph, Fig. 5, suggests their adsorption energies are respectively of the order of -72 and -68 kJ mol^{-1} for $Pt_{0.9}Rh_{0.1}$ and $Pt_{0.9}Ir_{0.1}$. The method is sufficiently precise to resolve the charge difference between different alloys, even when the 2nd element is present in a small percentage, and therefore to give a reasonable estimate of the

View Article Online
DOI: 10.1039/C6CP00106H

adsorption energies. Such energies are hard to estimate theoretically because of complexities such as preferential binding to one of the metals so our experimental approach is a particularly useful alternative. To account for variations in the theoretical adsorption energies arising from different DFT approaches,[27-31] Fig. 5 includes an error bar for the theoretical adsorption energies (from -84.9 to -79.1 kJ mol^{-1}) found in the literature for oxygen on Pt(111) fcc sites. All are in very good agreement with the experimental value. For the other metals considered here we have not found alternative theoretical calculations to the results reported in ref.[27] Although it is difficult to compare microelectrode experiments with gas phase experiments, it is nevertheless interesting to note that for the metal with the strongest binding strength, Ni, the experimental adsorption energy obtained with the Ni microdisc is in reasonable agreement with the average value (circa 210 kJ mol^{-1}) determined by calorimetry for oxygen adsorption on Ni(111) at 300 K and circa one third of a monolayer coverage.[14] However the limit of this comparison is shown for Pt(111) as gas phase experiments reveal larger adsorption energies, 115±8 kJ mol^{-1} at very low oxygen coverages,[14] than those observed with the Pt microdisc or than those predicted by the theoretical calculations.

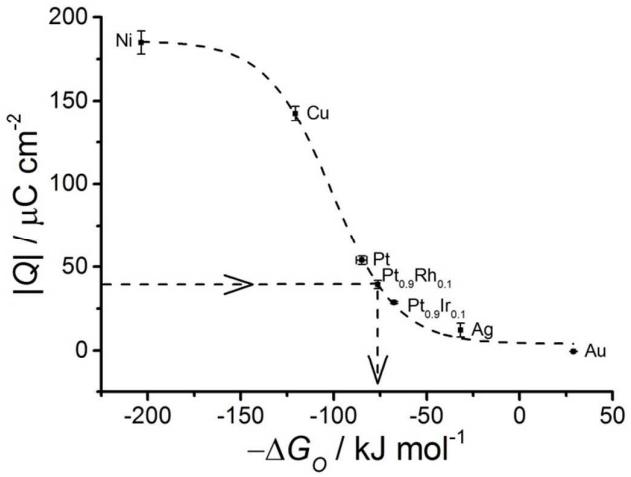

Fig.5: Charge calculated from the integrated difference between experimental and theoretical current transients for the oxygen reduction reaction at Ni, Cu, Pt, $Pt_{0.9}Rh_{0.1}$, $Pt_{0.9}Ir_{0.1}$, Ag and Au 25 μm Ø microdiscs in aerated 0.1 M $KClO_4$. The horizontal axis shows the theoretical adsorption energy of oxygen for the respective metals obtained from ref.[27] For Pt the adsorption energies are taken from ref.[27-31] The line is drawn as a guide to the eye. The arrowed line indicates how adsorption energies may be predicted using the guideline. Vertical error bars are the largest difference between the charges and the average for five current transients.

We now illustrate another way of exploiting the charge associated with the reduction of oxygen species adsorbed on the electrode. Since theoretical calculations predict that the kinetics of the oxygen reduction reaction is linked to the coverage of oxygen containing species,[6, 12] we investigated whether there is a correlation between the kinetic current for the ORR and the charge passed to reduce the adsorbed oxygen species. The ORR current was measured at 0.45 V vs. RHE on sampled current voltammograms[13, 20] to ensure every point was recorded with the same electrode history and in the same conditions as those used to record the charge. The current was normalised to account for the effect of mass transport (details are given in ESI†). In Fig. 6, blue curve, we first report the dependence of the ORR current on the theoretical adsorption energy between oxygen and the metal atoms; interestingly an almost identical curve is seen when plotting the kinetic current against the adsorption energies calculated from the stripping peaks. The curve shows a classical asymmetric volcano plot consistent with previous reports.[6, 9, 27] As expected the three platinum metals have the largest activity but the highest rate is obtained with the $Pt_{0.9}Rh_{0.1}$ microdisc. In contrast the green curve shows the dependence of the ORR current on the charge for the reduction of the oxygen species adsorbed on each electrode. There too we observe an asymmetric volcano plot but it is almost the mirror image of the blue curve. What is remarkable is that the green curve derives entirely from experimentally measured values. The reason behind the symmetry between the two curves is the unique relationship between the coverage of oxygen species (the charge) and their adsorption energy with the underlying metal previously shown in Fig. 4 and reproduced in red in Fig. 6. These results demonstrate a clear correlation between the kinetic ORR current at a given electrode and the charge associated with the reduction of adsorbed oxygen species on this electrode. Although this is in agreement with theoretical prediction, such correlation has, to our knowledge, not been previously observed experimentally.

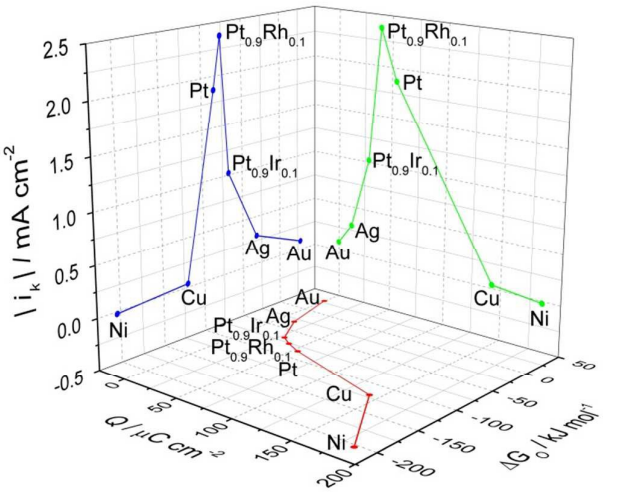

Fig.6: Dependence of the ORR kinetic current on the charge passed to reduce the adsorbed oxygen species (green) and on the theoretical adsorption energy of oxygen for the metal taken from ref.[27] (blue). Data from Fig. 4 (red).

Conclusion

This study has shown that the adsorption of oxygen species resulting from exposure to dissolved oxygen is very sensitive to the metal substrate and that a unique relationship exists between their coverage and their adsorption energy towards the substrate. The adsorption energies derived experimentally

View Article Online
DOI: 10.1039/C6CP00106H

are in remarkable agreement with the theoretical adsorption energies obtained with DFT despite the assumptions made in the theoretical models (e.g. defect-free, smooth, single crystal surfaces without repulsion between adsorbates). This merits further investigation but already it is clear that through a simple calibration curve, the charge associated with the reduction of the oxygen species can be used to predict their adsorption energy on complex substrates such as alloys. This is useful for the development of novel oxygen reduction catalysts as adsorption energy is often used as a descriptor for the activity of the catalyst. More importantly this study has revealed a clear correlation between the ORR activity and the coverage of oxygen species. The experimental volcano plot obtained when plotting the kinetic ORR current against the charge passed to reduce the oxygen species is akin to previously reported theoretical plots of catalytic activity against adsorption energy. These results clearly demonstrate that the charge recorded when reducing the adsorbed oxygen species can be used as a descriptor for the catalytic activity of the surface towards the ORR. These observations were made possible thanks to the unique properties of microdisc electrodes; we are now extending this work to real fuel cell catalysts. In conclusion this work has provided new insight into the oxygen reduction reaction and has demonstrated a new methodology to investigate the activity of a metal electrode towards the ORR.

Acknowledgements

S.C.P. acknowledges the support of the Faculty of Natural and Environmental Sciences, University of Southampton. The authors acknowledge Prof. Philip Bartlett and Derek Pletcher for many enlightening discussions.

References

1. N. M. Markovic, T. J. T. J. Schmidt, V. Stamenkovic and P. N. Ross, *Fuel Cells*, 2001, **1**, 105-116.
2. H. S. Wroblowa, Y. C. Pan and G. Razumney, *J. Electroanal. Chem.*, 1976, **69**, 195-201.
3. E. Yeager, *Electrochim. Acta*, 1984, **29**, 1527-1537.
4. A. M. Gomez-Marin and J. M. Feliu, *Chemsuschem*, 2013, **6**, 1091-1100.
5. A. M. Gomez-Marin, R. Rizo and J. M. Feliu, *Catal. Sci. Technol.*, 2014, **4**, 1685-1698.
6. H. A. Hansen, V. Viswanathan and J. K. Norskov, *J. Phys. Chem. C*, 2014, **118**, 6706-6718.
7. G. S. Karlberg, J. Rossmeisl and J. K. Norskov, *Phys. Chem. Chem. Phys.*, 2007, **9**, 5158-5161.
8. N. M. Markovic, H. A. Gasteiger and N. Philip, *J. Phys. Chem.*, 1996, **100**, 6715-6721.
9. J. Rossmeisl, G. S. Karlberg, T. Jaramillo and J. K. Norskov, *Faraday Discuss.*, 2009, **140**, 337-346.
10. J.-M. Noël, A. Latus, C. Lagrost, E. Volanschi and P. Hapiot, *J. Am. Chem. Soc.*, 2012, **134**, 2835-2841.
11. M. Zhou, Y. Yu, K. Hu and M. V. Mirkin, *J. Am. Chem. Soc.*, 2015, **137**, 6517-6523.
12. S.-P. Lin, K.-W. Wang, C.-W. Liu, H.-S. Chen and J.-H. Wang, *The Journal of Physical Chemistry C*, 2015, **119**, 15224-15231.
13. S. C. Perry and G. Denuault, *Physical chemistry chemical physics : PCCP*, 2015, **17**, 30005-30012.
14. W. A. Brown, R. Kose and D. A. King, *Chemical Reviews*, 1998, **98**, 797-832.
15. J. L. Gland, B. A. Sexton and G. B. Fisher, *Surf. Sci.*, 1980, **95**, 587-602.
16. J. Schmidt, C. Stuhlmann and H. Ibach, *Surf. Sci.*, 1993, **284**, 121-128.
17. J. Omura, H. Yano, D. A. Tryk, M. Watanabe and H. Uchida, *Langmuir*, 2014, **30**, 432-439.
18. J. Omura, H. Yano, M. Watanabe and H. Uchida, *Langmuir*, 2011, **27**, 6464-6470.
19. M. Sosna, G. Denuault, R. W. Pascal, R. D. Prien and M. Mowlem, *Sensors and Actuators B: Chemical*, 2007, **123**, 344-351.
20. S. C. Perry, L. M. Al Shandoudi and G. Denuault, *Anal. Chem.*, 2014, **86**, 9917-9923.
21. K. Stulik, C. Amatore, K. Holub, V. Marecek and W. Kutner, *Pure Appl. Chem.*, 2000, **72**, 1483-1492.
22. R. J. Forster and T. E. Keyes, in *Handbook of Electrochemistry*, ed. C. G. Zoski, Elsevier, Amsterdam, 2007, ch. 6, pp. 155-188.
23. P. J. Mahon and K. B. Oldham, *Anal. Chem.*, 2005, **77**, 6100-6101.
24. H. Angerste, B. E. Conway and W. B. A. Sharp, *J. Electroanal. Chem.*, 1973, **43**, 9-36.
25. X. C. Jiang, M. Seo and N. Sato, *J. Electrochem. Soc.*, 1991, **138**, 137-140.
26. Y. F. Yang and G. Denuault, *J. Chem. Soc.-Faraday Trans.*, 1996, **92**, 3791-3798.
27. J. K. Norskov, J. Rossmeisl, A. Logadottir, L. Lindqvist, J. R. Kitchin, T. Bligaard and H. Jonsson, *J. Phys. Chem. B*, 2004, **108**, 17886-17892.
28. P. C. Jennings, H. A. Aleksandrov, K. M. Neyman and R. L. Johnston, *Phys. Chem. Chem. Phys.*, 2014, **16**, 26539-26545.
29. Y. G. Suo, L. Zhuang and J. T. Lu, *Angew. Chem. Int. Ed.*, 2007, **46**, 2862-2864.
30. M. P. Hyman and J. W. Medlin, *J. Phys. Chem. B*, 2005, **109**, 6304-6310.
31. T. Li and P. B. Balbuena, *J. Phys. Chem. B*, 2001, **105**, 9943-9952.